RICCI CURVATURE AND FLOW FOR IMAGE DENOISING AND SUPER-RESOLUTION

Eli Appleboim, Emil Saucan, and Yehoshua Y. Zeevi

EE., Math., EE. Department, Technion – Israel Institute of Technology
Technion City, 32000, Haifa, Israel
phone: + 972-48294723, fax: + 972 -48294727, email: eliap,semil,zeevi@ee.technion.ac.il
web: www.visl.technion.ac.il

ABSTRACT

A discrete version of the Ricci flow, applicable to images, is introduced and applied in image denoising and in single-image-based enhancement and super-resolution. This flow is unique among the geometric flows that have been applied in image processing, in that it is the only flow wherein the metric of an image evolves rather than the image itself as is the case in other geometric flows applicable in image processing. The flow is based on the combinatorial Ricci curvature defined by Forman, that was previously introduced by the authors in the context of image processing. It is shown that the Ricci flow preserves image structure much better than the Beltrami flow and other state-of-the-art image enhancement schemes. Implementation of the Ricci flow is applicable also to general surfaces such as required in computer graphics and other applications.

1. INTRODUCTION

Diffusion methods, and curvature flows, based on the mean curvature of an image, considered as a surface embedded in some Euclidien space, belong by now to the basic repertoire of methods available to the image processing community (see, e.g. [23], [1], [14], [21], [22], [23], [24] and references therein). Typically, these flows come in the following form:

$$\frac{\partial I}{\partial t} = \mathscr{O}(I)\,, \tag{1}$$

where $\mathscr{O}$ is some operator, sensitive to curvature, acting on the image I. Recent years studies show that such flows are instrumental in applications such as reconstruction, segmentation and recognition (e.g. [6], [19], [25], [14], [1]).

One curvature function that is extensively used in geometry is the Ricci curvature. It measures the deviation of a manifold from being locally Euclidean in various tangential directions. More precisely, it appears in the second term of the formula for the $(n-1)$-volume $\Omega(\varepsilon)$ generated within a solid angle (i.e. it controls the growth of measured angles):

$$\mathbf{v}\cdot Ricci(\mathbf{v}) = \frac{n-1}{vol\left(\mathbf{S}^{n-2}\right)}\int_{\mathbf{w}\in T_p(M^n),\,\mathbf{w}\perp\mathbf{v}} K(<\mathbf{v},\mathbf{w}>)$$

where $<\mathbf{v},\mathbf{w}>$ denotes the plane spanned by $\mathbf{v}$ and $\mathbf{w}$, and $K(<\mathbf{v},\mathbf{w}>)$ is the sectional curvature relative to that plane via the exponential map. i.e. Ricci curvature represents an average of sectional curvatures. The analogy with mean curvature is further emphasized by the fact that Ricci curvature behaves as the Laplacian of the metric (see [4]).

The Ricci flow is defined by the following equation (see [11], [12]):

$$\frac{\partial \mathscr{G}}{\partial t} = -Ric(I)\,, \tag{2}$$

where $\mathscr{G}$ is the image metric and Ric denotes the Ricci curvature. The Ricci flow was proposed by Hamilton in [11] as a way of resolving some essential conjecture about the geometry and topology of 3-dimensional manifolds. Note that the flow given in Eq. (2) is essentially different from classical diffusion processes applied to images, such as Eq. (1), since in the Ricci flow it is the metric of the image rather than the image itself that is evolved. It is important to note that in dimension $n = 2$, which is the most relevant to classical image processing and its related fields, Ricci curvature equals twice the Gauss curvature.

Stimulated by Perelman's work on the Ricci flow ([16], [17]), some discrete versions of it penetrated the main stream of imaging and graphics, originating with the works of Gu et. al. [26].

In the work of Forman [8], combinatorial analogue of Ricci curvature is defined. This operator is introduced in [8] in the context of cell complexes. Roughly speaking, one can think of a grid, mesh or triangulation as examples of cell complexes. Every Riemannian manifold possesses a cell complex structure (see [15]).

The paper is organized as follows. In Section 2 we outline our proposed adaptation of the combinatorial Ricci curvature, as defined by Forman, to images. This adaptation was introduced in details by the authors in [20]. In Section 3 we use this operator for a novel diffusion process implemented on images, in the context of image enhancement. In Section 4 we present some experimental results. Finally, Section 5 summarizes the paper and presents some work in progress.

2. APPLICATIONS - FROM RIEMANNAIN MANIFOLDS TO IMAGES

In this section we briefly outline our proposed implementation of the Ricci curvature for images, following [20]. Before defining this curvature measure we have to introduce the cellular decomposition we attach to images. This comes natural, as it is induced by the *grid* representation of an image (illustrated in Figure 1). One should bear in mind that since we represent images as manifolds (usually surfaces), we need the cellular decomposition to be defined on the image surface. In this context, the 2-cells are actually the surface elements of the form $I(p)$, where $p = (i, j)$ is the (i, j) pixel of the image I, and the 1-cells are the arcs $I(e)$, where e is either vertical or horizontal edge between adjacent pixels.

© EURASIP, 2012 - ISSN 2076-1465

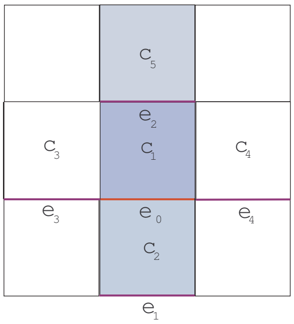

Figure 1: Cell decomposition of an image.

2.1 Ricci Curvature

Refering to the cellular structure imposed on images as described above, we define:

Definition 1. *The Ricci curvature of I along the edge e_0 is given by:*

$$\mathrm{Ric}(e_0) = w(e_0)\Big[\Big(\frac{w(e_0)}{w(c_1)} + \frac{w(e_0)}{w(c_2)}\Big) - \Big(\frac{\sqrt{w(e_0)w(e_1)}}{w(c_1)} + \frac{\sqrt{w(e_0)w(e_2)}}{w(c_2)}\Big)\Big] .$$

All terms w represent weight functions ([8]). These functions are supposed to reflect geometric entities such as length and area.

2.2 Weighting Methods

In this subsection we address the issue of how to determine the weights. We review two essential schemes for weighting, a combinatorial one and a geometric one. While it is unlikely to have an optimal set of weights, the geometric scheme seems to be superior over the combinatorial one in terms of quality of obtained results. However, it is more expensive in terms of computing resources.

2.2.1 Combinatorial weighting

In this case the weight $w(c)$ of a 2-cell surface element is assigned as the gray level of the corresponding pixel. The difference of gray levels of adjacent pixels along an edge e is taken as $w(e)$. Figure 2 depicts an example of Ricci curvature obtained with combinatorial weights.

2.2.2 Geometric Weights

While combinatorially weighting of cells is simple and efficient computationally, we would still like to account also for the geometry of the image. The most natural way to accomplish it is by defining the weights $w(e)$ and $w(c)$ so that they reflect length and area respectively. The basic way to do it is through the metric of the image. The metric of a gray level image is given by the matrix, ([21], [14], [22]):

$$\mathscr{G}_{i,j} = \begin{pmatrix} \beta + I_x^2 & I_x I_y \\ I_y I_x & \beta + I_y^2 \end{pmatrix} ,$$

where β is a parameter that scales the differential change of the image dI with respect to the spatial differentials of X and Y, dX, dY respectively, thus enabling one to adjust the sensitivity to image gradient (i.e. presence of edges - see [21]). For color images rendered as surfaces embedded in $\mathbb{R}^5$ with coordinate system $I = (X, Y, R(X,Y), G(X,Y), B(X,Y))$, a similar parameterized metric is given (see [21]).

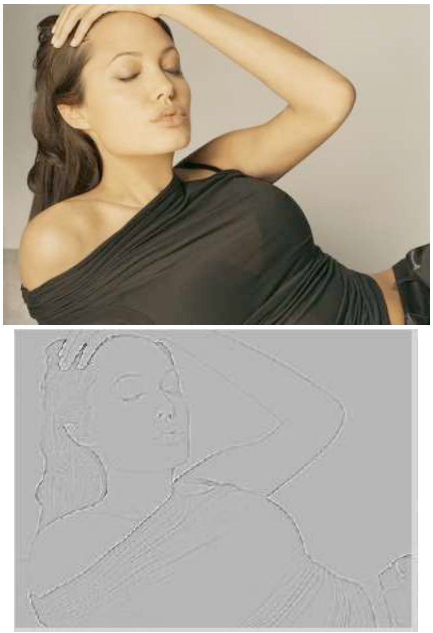

Figure 2: Ricci curvature obtained with combinatorial weights.

For simplicity, in this work we account for the "stretch" only in the horizontal and vertical directions. We therefore define:

$$w(e_x) = ds(e_x) = \sqrt{\beta + I_x^2}dx \, , \; w(e_y) = ds(e_y) = \sqrt{\beta + I_y^2}dy \, .$$

The area element above a pixel is then given only as first order approximation by $dA = ds(e_x)ds(e_y)$.
Figure 3 shows the outcome of computing Ricci curvature of an image, while using geometric weights.

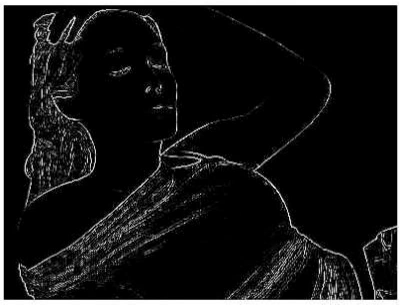

Figure 3: Ricci curvature with geometric weights. Notice the explicit detection of edges. This should be expected, since edge curvature is expected to be of significantly higher value than the value of curvature in homogenous areas.

3. RICCI FLOW FOR IMAGES

3.1 Classical Image Diffusion

The most common operators used for $\mathscr{O}$ in Eq. (1) are modifications of the Laplacian of the image, $\triangle I = tr(\text{Hess}I) = I_{xx} + I_{yy}$.
In the simplest linear case one assigns:

$$\mathscr{O} = \triangle I \, .$$

When considering images as Riemannian manifolds, it is common to replace the Laplacian by the Laplace-Beltarmi operator ([14], [22], [24]). One then set ([4], [18]):

$$\mathscr{O} = \triangle_{\mathscr{G}} I = \frac{1}{\sqrt{det(\mathscr{G})}} \sum_{i,j=1}^{2} \frac{\partial}{\partial X^i} \left(\sqrt{det(\mathscr{G})} \mathscr{G}^{i,j} \frac{\partial I}{\partial X^j} \right) .$$

It should be noted that $\triangle_{\mathscr{G}} I$ is exactly the mean curvature of the image surface (see [4]).

3.2 Ricci Flow

We are interested in applying the Ricci flow of Eq. (2) on images. Note again that in this case the metric of the image is evolved rather than the image itself. In particular, since the metric of an image is roughly equivalent to its gradient field, evolving the metric is equivalent to evolving the gradient field of the image. In order to be able to obtain a flow over the image it is therefore essential to solve the problem of reconstruction of an image out of its gradient field. The application of the Ricci flow on images is illustrated in the following diagram:

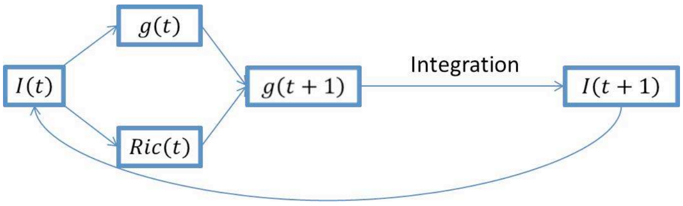

Figure 4: The Ricci flow diagram. Integration means that the newly iterated image is reconstructed from the evolved gradient field.

3.3 Image Reconstruction from Gradient Field

As noted above the reconstruction from the gradient field is essential for our scheme. We have used the method of Poisson solver proposed in [2]. In order to overcome noisy artifacts that are parts of the outcome of using the Poisson solver method, we use a Gaussian filter and apply it on the gradient field prior to applying the Poisson solver method. Figure 5 below shows the outcome of this method with and without filtering. Evidently, after smoothing the gradient field, the reconstructed image is smoother.

4. RESULTS

In all applications shown below weights where taken as geometric weights.

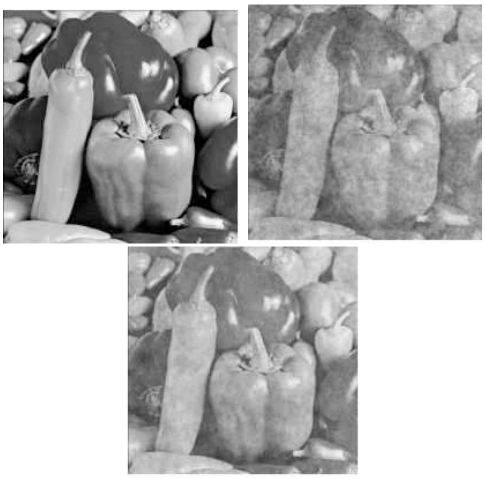

Figure 5: Reconstruction using Poisson solver. **Top left:** Original image. **Top right:** Reconstruction without filtering. **Bottom:** Reconstruction after Gaussian filtering of the gradient field.

4.1 Ricci Flow for Image Denoising

In Figure 6 we compare the performance of the Ricci flow with that of two other state-of-the-art denoising techniques. One is the Beltrami flow and the other is the non-local means method (see [22], [3]). The image shows Lenna with about 3.5 db of noise added to it. Note that in the noisy image, (Figure 6 top right), it is almost impossible to identify its content. Nevertheless, after just 3 iterations of the Ricci flow the content of the image clearly emerges. The Ricci flow significantly outperforms the other methods. This figure also illustrates an artifact of the flow under which the image is overall darker. This artifact is addressed in our current study in which we apply a normalized version of the flow that keeps the DC component of the image fixed. In Figure 7 we compare the performance of the Ricci flow with that of the Beltrami flow and of the total variation diffusion scheme for the task of denoising ultrasound images ([3]). The image shows part of the brain of a human embryo. Scrutinizing the bottom-right corner of the figure, it is observed that both the Beltrami and the Ricci flow overcome the speackle noise of the ultrasound better than the total variation scheme. However, the Ricci flow preserves the detailed structure of the image much better than the Beltrami flow. This is a direct consequence of the fact that by applying the Ricci flow on a surface that has the topology of a disk, the flow converges to a surface of strictly positive constant curvature (see [12]), which reflets a preserved structure of the image. This is in contrast with the case of Beltramy flow (or any other geometrical flow for this matter) wherein, by appllying it to such a surface, the outcome is a flat surface and, hence, no corresponding image structure is preserved.

4.2 Inverse Ricci Flow for Single Image Sharpening and Superresolution

Whereas the Ricci flow smoothes a surface until it converges to a surface of constant curvature (see [12]), the inverse Flow presented below is endowed with a sharpening effect. We use it in order to overcome blurring effects that are caused

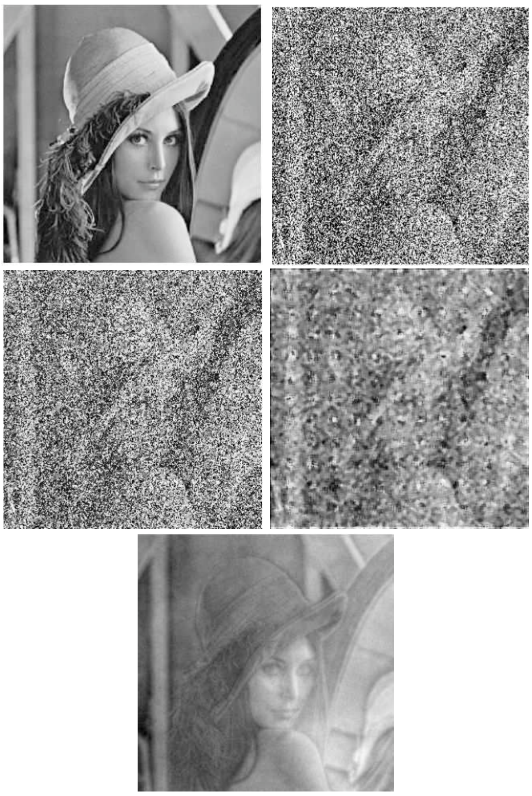

Figure 6: Ricci flow applied to Lenna image. **Top left:** Original image. **Top right:** Original image with 3.5 db noise. **Middle left:** Image after Beltrami flow. **Middle right:** Image after non-local means.**Bottom:** Image after 3 iterations of the Ricci flow. Note the fair reconstruction of the very noisy image.

by image interpolation. The inverse Ricci flow is given by:

$$\frac{\partial \mathcal{G}}{\partial t} = Ric(I)\,. \tag{3}$$

In Figure 8 we illustrate an image that underwent first a bicubic interpolation and then was sharpened by inverse Ricci flow. One can easily see how the edges of the interpolated image become smoother and the image looks sharper. Some non-continuousness artifacts can be seen along the edges. These artifacts are obtained due to the fact that the inverse Ricci flow is an ill-posed operator. We expect the normalized flow to reduce these artifacts.

5. SUMMARY

The Ricci flow, introduced in this paper in the context of image processing, is applicable to the processing of fully textured images in a variety of tasks such as enhancement. It is important to note that the Ricci flow is unique among flows that are applied in image processing, in that it is the only flow wherein the metric of an image evolves rather than the image itself, as is the case in other flows applicable in image processing. As a direct consequence of this important property, the evolutionary process converges onto a surface of constant, strictly positive curvature. This non-flat surface reflects a certain image-structure that is preserved under the flow. This is in contrast to all diffusion-type flows (including Beltrami), where the surface is flat in the limit (i.e. no image structure is preserved). Examples shown in the paper, and many more, show very high rate of convergence of the flow, achieving very good results already after only very few iterations. The results of the denoising process are shown to be superior to those obtained by other state-of-the-art methods. Normalization of the flow can easily preserve the DC level of the image and enable to overcome some of the artifacts of the non-normalized flow. We also implement the Ricci flow on video sequences. Implementation of the Ricci flow as suggested in this paper is also applicable for general surfaces such as those encountered in the context of computer graphics.

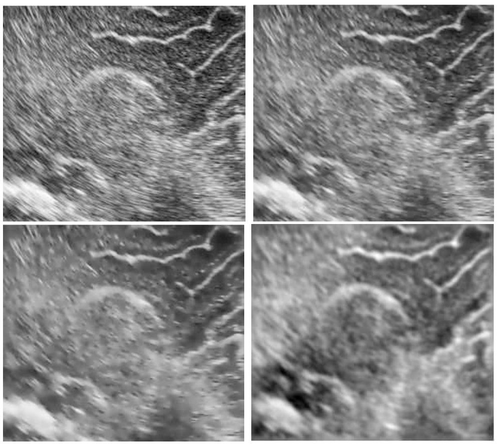

Figure 7: Ricci flow on real data. **Top left:** Original ultrasound image. **Top right:** Image after total variation filtering. **Bottom left:** Beltrami flow. **Bottom right:** Image after Ricci flow.

Acknowledgements The authors would like to express their gratitude to the students Nir Getter, Amitay Bar, Aviv Gadot and Aviram Haimovich for their devoted work while programming and implementing essential parts of the proposed methods.
Research was sponsored in part by the Ollendorf Minerva Center for Vision and Image Sciences.
Second author's research partly supported by the Israel Science Foundation and by European Research Council under the European Community's Seventh Framework Programme (FP7/2007-2013) / ERC grant agreement n^o [203134].

REFERENCES

[1] Angenent, S., Pichon, E. and Tannenbaum. A., *Mathematical Methods in Medical Image Processing*, Bulletin of AMS, 43, 3, 365-396, 2006.

[2] Agrawal, A., Raskar, R., and Chellappa, R., *What is the Range of Surface Reconstructions from a Gradient Field?*, ECCV 2006.

[3] A. Buades, B. Coll, J.M Morel, A review of image denoising algorithms, with a new one, SIAM Multiscale Modeling and Simulation, 4(2), 490-530, 2005.

[4] Berger, M. A., *Panoramic View of Riemannian Geometry*, Springer-Verlag, Berlin, 2003.

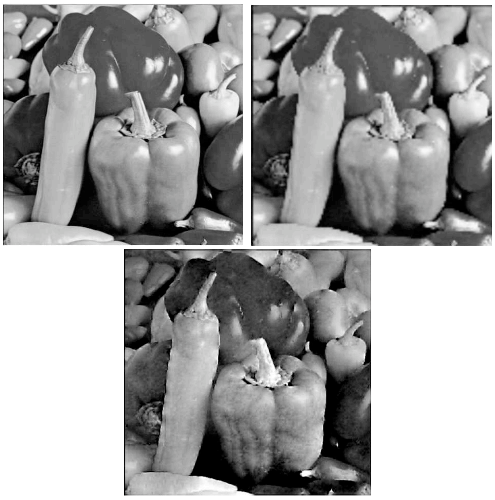

Figure 8: Inverse Ricci flow. **Top:** Original image. **Middle:** Image after bicubic interpolation. **Bottom:** Image after bicubic interpolation followed by inverse Ricci flow. Notice the sharped edges obtained by the flow.

[5] Chow, B. and Luo, F., *Combinatorial Ricci Flows on surfaces*, J. Diff. Geom. 63, 97-129, 2003.

[6] Dai J., Luo W., Yau S.-T. and Gu X., *Geometric accuracy analysis for discrete surface approximation*, Geometric Modeling and Processing, 5972, 2006.

[7] Fuster, A., Astola, L., and Florack, L., *A Riemannian Scalar Measure for Diffusion Tensor Images*, Proc. of CAIP 2009, LNCS 5702, 419426, Springer-Verlag, Berlin, 2009.

[8] Forman, R., *Bochner's Method for Cell Complexes and Combinatorial Ricci Curvature*, Discrete and Computational Geometry, 29(3), 323-374, 2003.

[9] Gilboa, G., Sochen, N. and Zeevi, Y. Y., *Forword and Backword Diffusion Processes fo Adaptive Image Enhancement and Denoising*, IEEE. Trans. Im. Proc., 2002.

[10] Gu, X. and Yau, S. T., *Global Conformal Surface Parameterization*, Proc. Eurographics Symposium on Geometry Processing (2003).

[11] Hamilton, R., *Three-manifolds with positive Ricci curvature*, J. Diff. Geom. 17, 255306, 1982.

[12] Hamilton, R., *The Ricci Flow on Surfaces*, A.M.S. Contemp. Math., 71, 1986.

[13] Jost, J., *Riemannian Geometry and Geometric Analysis*, Springer-Verlag, Berlin, 2002.

[14] Kimmel, R. Malladi, R. and Sochen, N., *Images as embedded maps and minimal surfaces, movies, color, textures and volumetric medical images*, Int. Jour. Comp. Vis., 39, 111-129, 2000.

[15] Milnor, J., *Morse Theory*, Ann. Math. Stud., 51, 1963.

[16] Perelman, G., *The entropy formula for the Ricci flow and its geometric applications*, arxiv:math.DG/0211159, 2002.

[17] Perelman, G., *Ricci flow with surgery on three-manifolds*, arxiv:math.DG/0303109, 2003.

[18] Petersen, P., *Riemannian Geometry*, Springer-Verlag, New York, 1998.

[19] Saucan, E., Appleboim, E., and Zeevi, Y. Y., *Sampling and Reconstruction of Surfaces and Higher Dimensional Manifolds*, J. Math. Im. Vis., 30(1), 105-123, 2008.

[20] Saucan, E., Appleboim, E., Wolansky, G. and Y. Y. Zeevi, *Combinatorial Ricci Curvature and Laplacians for Image Processing*, Proc. of CISP'09, Vol. 2, 992-997, 2009.

[21] Sochen, N. and Zeevi, Y. Y., *Representation of Colored Images by Manifolds Embedded in Higher-Dimensional Non-Euclidean Space*, IEEE. Proc. of ICIP98, 1998.

[22] Sochen, N., *Affine Invariant Flows in the Beltrami Framework*, J. Math. Imaging Vis., 20 133-146, 2004.

[23] ter Haar Romeny., B. M., (ed.), *Geometry-driven diffusion in computer vision*, Kluwer, Dordrecht, 1994.

[24] Weickert, J., *Anisotropic Diffusion in Image Processing*, ECMI Series, Teubner-Verlag, 1998.

[25] Yakoya, N. and Levine, M. *Range image segmentation based on dierential geometry: A hybrid approach*, IEEE Transactions on Pattern Analysis and Machine Intelligence, 11(6), 643-649, 1989.

[26] Yin, X. Jin, M. Luo, F. and Gu, X., *Discrete Curvature Flow for Hyperbolic 3-manifolds with Complete Geodesic Boundaries*, Proc. Symp. on Geom. Processing, Copenhagen, Denmark 2008.